5-2017

An in vitro study on the detection of ovarian cancer using a novel pH-specific targeting polypyrrole nanocontrasting agent.

Phillip Chuong
University of Louisville

An In Vitro Study on the Detection of Ovarian Cancer using a Novel pH-specific Targeting Polypyrrole Nanocontrasting agent

By
Phillip Chuong

Submitted in partial fulfillment of the requirements
for Graduation magna cum laude
and
for Graduation with Honors from the Department of Biology

University of Louisville

January, 2017

ABSTRACT

Longitudinal tracking and accumulation of polymeric nanoparticles in the context of cancer has largely occurred through identification of a fluorescent cargo. In this study, we created a dual extracellular acidic pH targeted polypyrrole-based hollow nanoparticle as a theranostic (maintain both therapeutic and diagnostic capabilities) agent for improved detection and treatment of ovarian cancer. Polypyrrole-hollow nanospheres (PPy-CS) were fabricated through the removal of a silver chloride (AgCl) core, which served as a template, followed by coating with chitosan and further tumor targeted with a pH low insertion peptide, V7. We exploited the NIR-absorbing property of polypyrrole to track both the nanoparticle separately from its NIR-fluorescent cargo. Utilizing the absorbing properties of the PPy-CS which contained an IR-780 cargo, multispectral optoacoustic tracking of phantom-based models revealed that both polypyrrole and IR-780 were separately identified indicating both the presence of the nanomaterial and cargo dye.

SUMMARY:

In this study, a nanoparticle was developed to serve as means to enhance the detection of ovarian cancer tumor cells *in vitro*. A unique feature of this nanoparticle was its ability to actively target the acidic microenvironment found in the extracellular matrix of all tumor cells. The nanoparticle was synthesized by utilizing a polymer-base and then encapsulated with chitosan and the modified targeting peptide. A series of characterization studies and assays were conducted to determine the effectiveness of the nanoparticle. Characterization studies demonstrated the nanoparticle displayed an appropriate size of approximately 50 nm. This size is small enough to not be detected by macrophage in the liver and large enough not to be effluxed out of the vasculature of the tumor microenvironment. Assays demonstrated the nanoparticle's ability to maintain its

cargo and actively target tumor environments with minimal off-targeting. The nanoparticle was placed in an optoacoustic tomographic imaging system to determine its ability to be tracked by the imaging system. The nanoparticle displayed signaling within the imaging system both with the infrared dye and alone.

1. INTRODUCTION

In the United States, ovarian cancer is the fifth leading cause of cancer-related deaths among women. Although only affecting approximately 1 out every 75 women, the 5-year survival rate is only approximately 17%. The reason for this rather low survival rate is due to the lack of earlier detection of ovarian cancer. Most women who are diagnosed with ovarian cancer are being diagnosed in later stages (III and IV) rather than the earlier stages (I and II), where treatment is much more beneficial and effective. The current imaging modalities utilized are those such as magnetic resonance imaging (MRI), computed tomography (CT), and positron emission tomography (PET). The lack of earlier detection stems from the inability for most imaging modalities to differentiate the presence of early stage ovarian tumors.

The current method of treatment consists of rounds of chemotherapy focused around the Enhanced Permeability Retention (EPR) effect. The EPR effect is the phenomenon in which molecules of certain molecules circulate through the body and eventually accumulate in tumor tissues much more so than in non-malignant areas. However, there are limitations to the effectiveness of this method of treatment. Most chemotherapeutics are highly cytotoxic, compounds harmful to living cells, and display harmful effects to non-malignant areas. Due to the problems current methods have faced, alternative treatment options have been developed to provide patients with better care.

The use of nanovehicles, targeting nanoparticles containing specified cargo, as a possible contrasting agent has shown great promise in substantially improving the detection and treatment of cancer [1, 2]. However, there still remain underlying problems and limitations to their effectiveness. The development of novel metallic-based nanovehicles utilizing receptor-targeting mechanisms has been extensively studied, due in part to the ability to track these metallic nanoparticles by means of nuclear imaging modalities and more recently optoacoustic imaging [3]. Unfortunately, the majority of metal components (Fe, Zn, Cu, Ti, Co, etc.) found in these nanoparticles exhibit some level of cytotoxicity. More specifically, the nanosized particles of these metal-oxides have recently shown to be toxic to some organisms [4]. Therefore, the use of polymer-based nanoparticles has garnered much attention as a possible theranostic tool in the treatment of cancer [5]. This interest is due to the low-cytotoxicity, controllable permeability, and surface functionality inherently found in polymer-based hollow nanospheres [6-8].

However, polymer-based nanoparticles themselves have encountered obstacles which have resulted in its further development as well. Difficulties in tracking polymer-based nanoparticles result from a general requirement of additional contrast dyes, radio-labels, or other tracking moieties to determine *in vivo* biodistribution and accumulation. With this in mind, a traceable compound, pyrrole, was selected to provide an encapsulation coat for cargo. Uniquely, polypyrrole polymers display an inherent absorbing property in which the pyrrole absorbs at the higher level of the spectrum, approximately 980 nm [9]. This inherent emittance of signal, by the pyrrole nanoparticle, allows for enhanced levels of tracking of the nanocontrasting agent, while *in vivo* with the use of optoacoustic tomography. Nanocontrasting agents serve as vehicles which contain contrast agents, such as dyes, that allow for better detection by an imaging modality. This polypyrrole chitosan-coated hollow nanosphere (PPy-CS Hollow Nanosphere) is unique

in the fact that it emits a photoacoustic signal without the aid of an additional NIR-dye cargo. From the research we have conducted, contemporary nanoparticles do not display any detectable absorbance properties which would allow for such enhanced detection. This nanoparticle, in unison with the emerging modality of optoacoustic imaging, can address many of the shortcomings of current diagnosis methods as well as enhance targeted drug delivery to tumor cells.

Currently, nuclear imaging is the foremost imaging modality used in terms of non-invasive in-situ imaging of biological tissues and materials. However, with the need for further improvement of image resolution and quality, optoacoustic imaging has emerged as a promising novel biomedical imaging modality [10, 11]. Unlike nuclear imaging, optoacoustic imaging does not solely utilize radio-labels and radioactive material [12] as a means to trace a contrasting agent, rather it emits light energy which then reflects off of the contrast agent and produces a sound wave which is then recorded by an ultrasonic transducer allowing for an ultrasound image with higher resolution [13-16].

Multispectral optoacoustic tomography (MSOT) combines the benefits of enhanced sensitivity found in optical imaging and the depth of detection that is usually associated with ultrasound [17]. The ability for detection without the need for application of radiation is a significant benefit due to the damaging side-effects associated with prolonged exposure to radiation [18, 19]. An advantage of MSOT imaging also includes its ability to compile molecular and functional information, with high spatial resolution, in real-time. Also, it is able to distinguish various contrasting agents already present within the tissue, e.g. hemoglobin [16, 18]. Due to optoacoustic imaging's ability to detect absorbing molecules at depth, it provides a means of detection for absorbing nanoparticles which would allow for determination of the overall accumulation and biodistribution in real time. In current mice models, this process occurs over a process of hours until the

nanoparticles are able to completely reach the tumor microenvironment. The advantages of optoacoustic imaging capabilities provide essential features including less exposure to radiation, rendering of more in-depth imaging, and a lesser invasive procedure than that of current modalities. Therein lies the need for the further development of enhanced tumor targeting agents [20-24].

In order for nanovehicles to be effective in the clinic, the nanovehicle must have: 1) increased tumor-specific accumulation and reduced off-target binding, and 2) increased signal/payload within tumors than compared to current diagnostic or therapeutic agents While additional biological barriers, e.g. poor vascularity [25] and presence of stroma [26], associated with recalcitrant tumors present additional challenges for development of nanovehicles, these recalcitrant tumors also offer the potential for high clinical impact for theranostic agents. Tumor-environments display various hallmark features which include acidic extracellular pH [27], increased levels of hypoxia [28], presence of autoantibodies [29] etc. With this in mind, we exploited the presence of acidic pH in the extracellular matrix of tumor cells as a general feature that would not be present in non-malignant tissue. In the clinic, tumors have acidic pH_e (6.4–6.8) compared to non-malignant tissue (pH_e 7.2-7.4) [30]; however, this small difference in extracellular pH alters the function, metastatic potential, and survival of tumor cells. To exploit the acidic extracellular pH as a targeting strategy for our polypyrrole nanocontrasting agent, we utilized a V7 pHLIP (pH Low Insertion Peptide), which changes conformation in response to its environment. In neutral pH_e (7.2-7.4), it maintains a globular form and transforms to a transmembrane alpha-helix at acidic pH_e conditions (6.4-6.8), this then allows the conjugated particle to insert and anchor into tumor cells [31-33].

pHLIPs are a specialized group of peptides derived from the bacteriorhodopsin C helix which maintain water solubility and semi-hydrophobicity. In neutral or higher pH

levels, the pHLIP is monomeric, remains non-reactive, and retains an unstructured or globular form. However, when placed in an acidic environment, it leads to the protonation of negatively charged residues on the helical segment and results in a shift in equilibrium, ultimately forming the alpha-helix structure [31]. Multiple studies have been successfully conducted with the use of pHLIPS as an additional modifier to existing polymer-based nanoparticles for pH-sensitive *in vivo* targeting for delivery as well as imaging [34, 35].

Recently, several types of ligand based probes and inorganic nanoparticles have been detected using optoacoustic imaging for improved cancer detection in glioma, breast, and pancreatic cancers [36]. Near-infrared(NIR) fluorescent dyes conjugated to tumor targeted ligands and gold nanomaterials (including nanorods, and gold composite nanostructures) are likely the most-widely explored exogenous contrast agents for optoacoustic imaging. A number of other inorganic nanomaterials, including gold and silver nanoparticles, have also demonstrated tumor specificity [6, 37], albeit often in subcutaneous tumors. However, the majority of inorganic nanoparticles have high uptake in the MPS system and may remain in the subject for long periods of time without the potential of degradation. This is a serious problem for the development of nanocontrasting agents for clinical use as patients often will receive multiple doses over time to determine tumor response, progression, and potentially even local metastasis. Therefore, the use of NIR absorbing organic nanoparticles offers a substantial improvement as nanocontrasting agents detectable by optoacoustic imaging.

In this study, I synthesized, modified, and evaluated an acidic extracellular pH-targeting polypyrrole chitosan-coated hollow nanosphere as a tumor targeting nanocontrasting agent detectable by multispectral optoacoustic tomography [38, 39]. With the addition of the V7 ligand to the PPy-CS, the nanoparticle displayed enhanced targeting capabilities *in vitro.* To the extent of my knowledge, this is the first

recorded tracking of a polymer-based nanoparticle through optoacoustic imaging in any ovarian cancer cell line, without the use of an additional contrasting agent. This nanoparticle is unique in the fact that the polypyrrole-coating provides an enhanced spectrum of detection through its inherent absorbance in the infrared region. The incorporation of this nanoparticle and fluorescent dye has proved to be a successful contrast agent and displays great promise for possible future use as a nanovehicle for chemotherapeutics.

2. RESULTS AND DISCUSSION

2.1 Particle Synthesis and Characterization

The schematic seen in Figure 1 displays the experimental method which was used to synthesize the PPy-CS. From transmission electron microscopy (TEM) analysis (Figure 1B), we were able to confirm the successful removal of the AgCl cores as well as the desired relatively small-size of 43.56 ± 9 nm in diameter with a pore-size of 15 ± 6 nm (This size is approximately equivalent to the eye-lash of Abraham Lincoln on the penny). Nanoparticles with a size greater than 100 nm tend to be too large and would eventually be filtered out by macrophage found in the liver or kidneys [40]. Therefore, particle size control played a crucial part during the synthesis of these particles.

Figure 1:

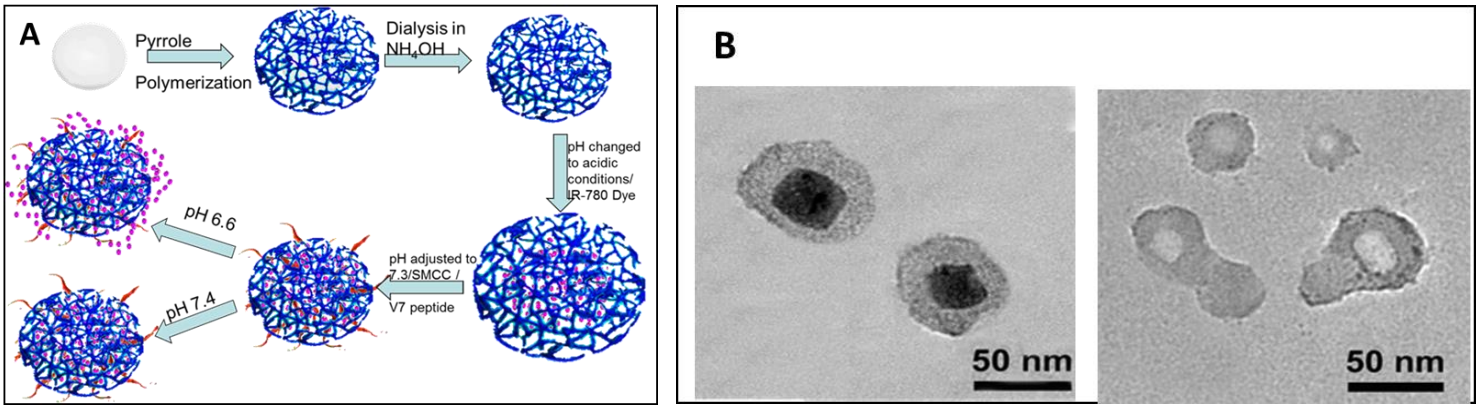

Additionally, particle size was confirmed with the use of dynamic light scattering (DLS) [41]. Figure 2 displays the DLS measurement of the PPy-CS maintaining a particle size of 51.39 nm. This measurement was slightly larger than the desired range of less than 50 nm; however, it remained consistent with the readings from the TEM images. This desired size was obtained through a series of dialysis in ammonium hydroxide and modified measurements of the initial substrates to form the silver-chloride core.

Figure 2:

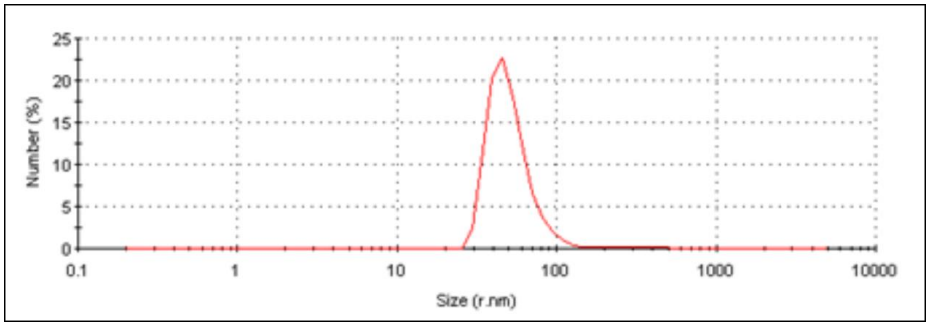

Zeta potential was incorporated to measure the change in voltage exhibited by the nanosphere [42]. Zeta potential is utilized in determining the potential difference between a solid surface of a particle and its conducting solvent. This technique was used to help determine the expansion of the chitosan-coat in the presence of acidic pH and to ensure

encapsulation in the presence of more neutral pH. The zeta potential of the nanospheres in various pH displayed a difference of -12.4 to -9.6 (Figure 3). An increase in voltage was seen as the corresponding pH decreased [43, 44]. As pH decreased, the attraction/stability between the pyrrole-coating and chitosan increased and resulted in enhanced binding with regards to pH-specificity. These results confirmed the formation of the nanosphere with a functional chitosan-coat.

Figure 3:

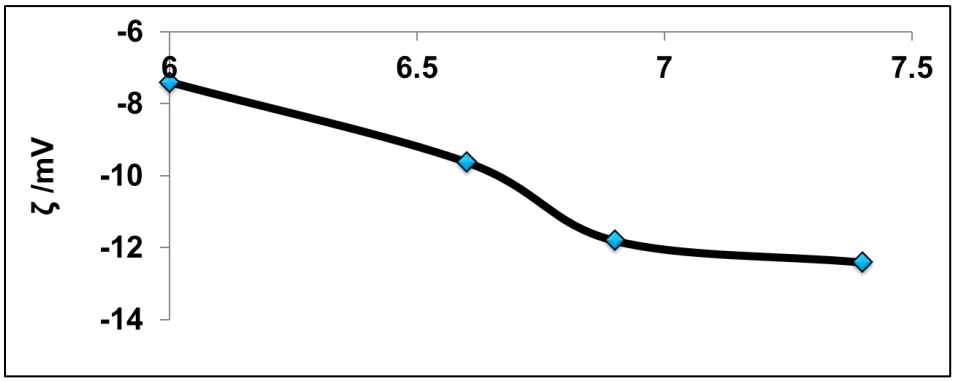

The absorbance properties displayed by the PPy-CS, alone, allowed for detection using MSOT without the aid of a dye or any other indicator. This inherent absorbance signal provides a significant advantage to the further development of tumor-targeting nanocontrasting agents. To the best of our knowledge, we believe this is the first study that depicts the tracking ability of a polymer particle without the aid of an additional contrasting agent by means of optoacoustic imaging. With the aid of the MSOT system, we were able to determine that the synthesized nanosphere displayed its own unique absorbance signal which was distinguishable from the IR-780 dye (Figure 4). The pyrrole, alone, emitted a signal greater than 800 nm and extended onward, while the PPy-CS hollow nanospheres emitted a peak at 710 nm (Figure 5).

Figure 4:

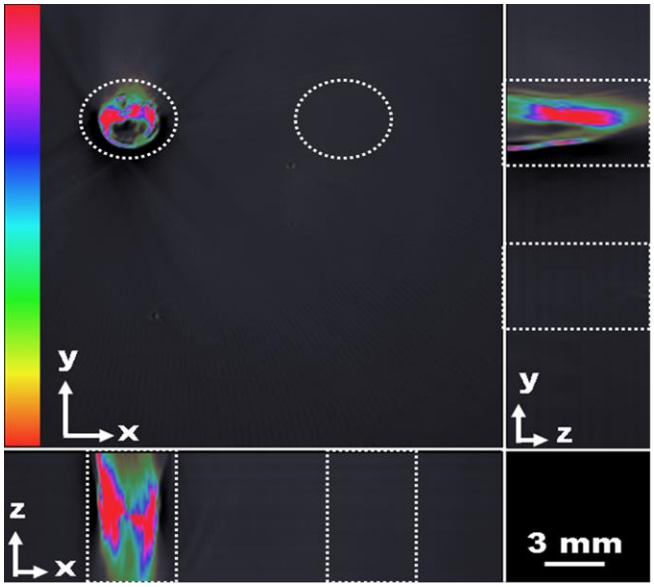

Figure 5:

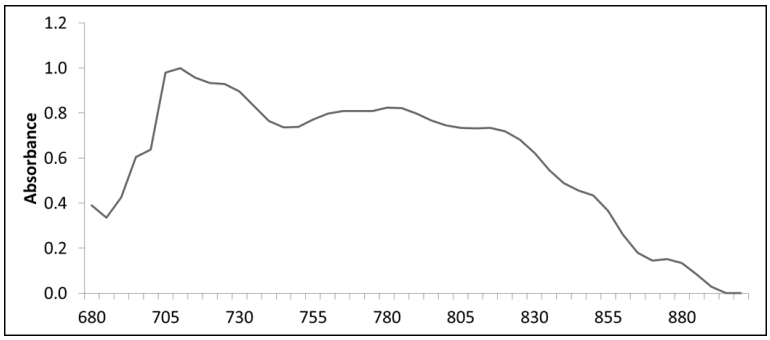

With increased ability to ascertain the biodistribution of the nanospheres and dye separately, we were better able to track the efficiency of the nanoparticle's tumor-targeting capabilities. The development of a nanocontrasting agent with the ability for detection, without the limitation of a dye, enables for enhanced detection as well as further insight in the trajectory and effectiveness of delivery of chemotherapeutics. This unique property may prove to be a strategic indicator in future studies and possibly minimize inexact/inconclusive signaling.

2.2 Determination of pH specificity of V7-conjugated PPy-CS hollow nanospheres *in vitro*

Two ovarian cancer cell lines, ES-2 and A2780, were utilized to determine cellular uptake of the nanoparticles. ES-2 cell lines are an aggressive cell line and are typical in patients who are diagnosed with later stage ovarian cancer. A2780 cell lines are not as aggressive, but are a type found in many patients diagnosed with ovarian cancer as well. The nanoparticle, containing IR-780 dye, was introduced to both cell lines and placed on a rocker in a non-CO2 incubator to allow for distribution of the particle throughout the well. A non-CO2 incubator was utilized in order to prevent possible changes in the pH of the media, if it were to interact with carbon-dioxide. The plates were then placed on odyssey infrared imaging to determine uptake of the nanoparticles in the cells. For both cell lines, greater uptake was observed in the more acidic environments, pH 6.6, compared to those in neutral, pH 7.4. For the A2780 cell line, binding was approximately 9.3 times greater for the corresponding pH levels. For the ES-2 cell line, binding was approximately 7 times greater in pH 6.6 compared to 7.4. (Figure 6).

Figure 6:

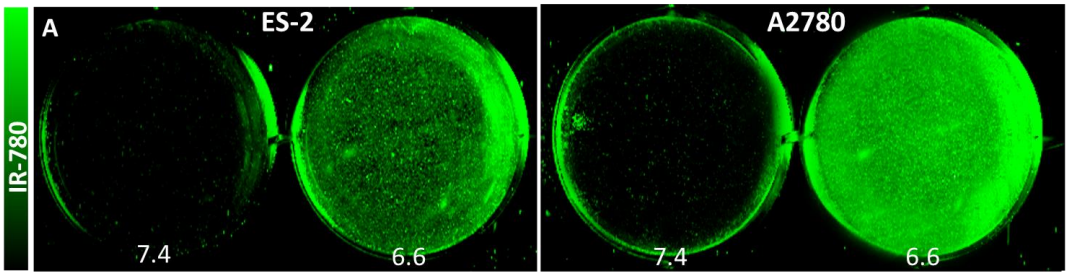

Figure 6:

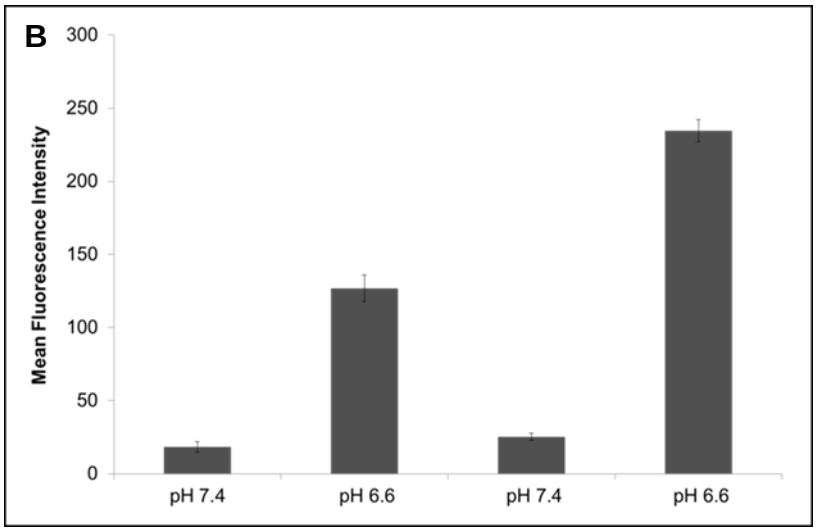

Tissue-phantoms were used to further test the pH-specificity of the dye-conjugated PPy-CS. Two separate conjugation processes were used to determine which displayed a greater level of binding, with regards to acidic pH. (3-Aminopropyl) triethoxysilane (APTES) is utilized as a cross-linker, which aids in the binding of the peptide-linker, 4-(*N*-Maleimidomethyl)cyclohexanecarboxylic acid *N*-hydroxysuccinimide ester (SMCC) to the surface of the nanoparticle. APTES is needed in order to fully conjugate the V7-peptide to the nanoparticle. The introduction of APTES in the early conjugation process displayed 3.5 times greater binding intensity at pH 6.6 compared to pH7.4. This earlier addition occurred after the encapsulation of the dye. The later addition occurred after the addition of SMCC. However, the addition of APTES at the later stages of conjugation displayed 9.4 times greater binding intensity for the corresponding pH (Figure 7). This variation in APTES addition may display the role of the linker as a more efficient intermediary agent for the addition of SMCC compared to its role in the conjugation of chitosan.

Figure 7:

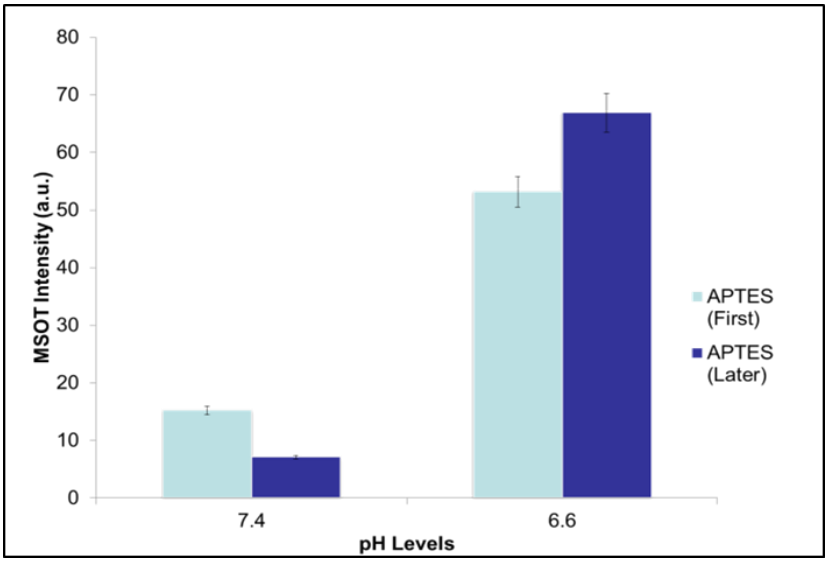

2.3 Cellular uptake of PPy-CS

To further determine the pH specificity of the PPy-CS, fluorescence microscopy was performed to verify whether or not the PPy-CS were truly being anchored into the tumor cells [45]. Propidium iodide was utilized as the contrasting agent. Because Propidium iodide is not a cell permeable dye, it was encapsulated into the nanospheres in order to monitor the intracellular uptake and dye release in conjunction with acidic pHe. The fluorescence of red compared to green confirmed whether cellular uptake or accumulation on the surface was taking place.

2.4 Dye-Release Assessment of Cargo-Carrying Capability

PPy-CS loaded with IR-780 dye were evaluated for pH-specific dye release. The dye-conjugated nanoparticles were introduced into phosphate buffer saline (PBS) solutions of pH 6.6, 6.9, or 7.4. The PPy-CS in PBS solution of pH 6.6 were found to have released ~1.7 times greater the amount of IR-780 dye compared to those in PBS solution of pH 6.9 and 7.4 (Figure 8). It was determined that the level of absorbance directly correlated with the amount of IR-780 dye that had been released from the PPy-CS [46].

This contrast in dye release illustrates the preferential release of cargo displayed by the PPy-CS. From these dye-release kinetics, it can be inferred that introduction of the nanospheres *in vivo* will result in targeted release of cargo to the tumor-region and limited off-targeting to non-malignant tissue. In a clinical setting, the nanovehcles, containing the infrared dye, is detected with a handheld scanner and the image is then seen on the optoacoustic system. This provides a less-invasive and more accessible method of imaging than compared to current methods.

Figure 8:

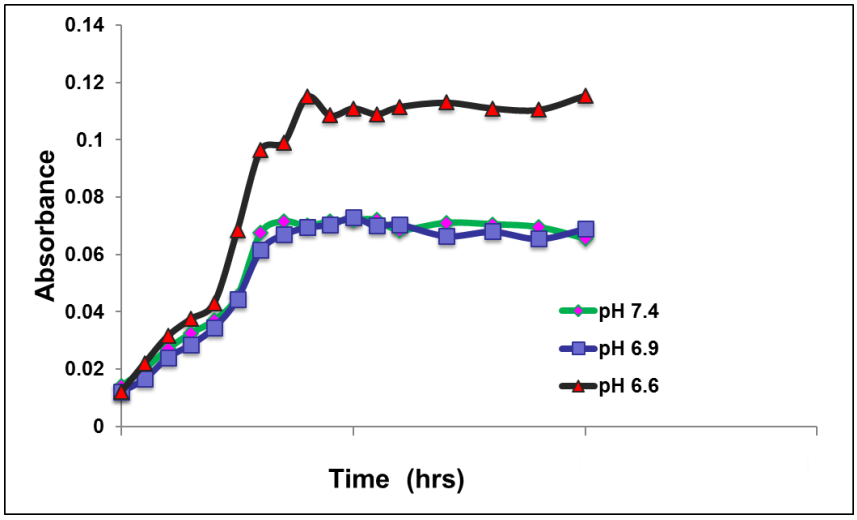

The pyrrole-coating provided a flexible structure which allowed for the nanosphere to better conform to its surroundings [47]. The PPy-CS were better-equipped to adapt to the change from neutral pH to more acidic pH without fracturing the overall integrity of the structure and pre-maturely releasing its cargo. The chitosan-coating expanded, in the presence of acidic pH, and released the dye. However, in the presence of neutral pH, the chitosan-coating would remain intact and continue to encapsulate the dye. This specified targeting and specified release helped to prevent off-targeting. The PPy-CS, carrying dye, required a rate of release that was not immediate and random, but discharged at a rate in which a majority of the dye was gradually released in the tumor-region.

3. CONCLUSION

In this study, pyrrole exhibited inherent absorbance properties which allowed it to be detected without the aid of a contrasting dye. This distinction would allow for a more precise tracking of the targeted nanosphere *in vivo.* With pyrrole serving as the principal encapsulating vehicle, a hollow nanosphere with a dual pH-specific mechanism was developed using a silver-chloride core template with pyrrole and chitosan-coating. It was then conjugated with a specifically designed pH-specific reactive ligand to allow for tumor-targeting. Conjugated PPy-CS displayed active tumor-targeting capabilities in *in vitro* studies with limited off-targeted binding. The use of a pyrrole-based nanoparticle incorporated with fluorescent dye has presented itself as a novel nanocontrasting agent. The nanoparticle demonstrated a sufficient size of ≈ 44 nm with a pore size of ≈ 15 nm. This target size allows for efficient uptake by tumor cells without the disadvantageous side-effects of larger particles such as targeting by macrophage in the kidneys. These dimensions are most suitable for transport and navigation towards the tumor cells once intravenously introduced.

Using various imaging modalities, we further evaluated the biodistribution and tracking of the PPy-CS and established that the nanospheres exhibited amplified signaling and pH specificity. This unique inherent absorbance displayed by the PPy-CS allowed for enhanced detection of the nanosphere by the imaging system. The inherent absorbance provided an individual spectrum which allowed for a distinction between the actual nanoparticle and the location of the IR-780 dye. Being able to distinguish the location of the separate components allowed for a more accurate interpretation of the effectiveness that the nanoparticle would display in locating the desired tumor-region.

In future studies, the PPy-CS will be functionalized to serve as nanocarriers for chemotherapeutics due to its unique tracking capabilities in photoacoustic imaging. Additional modifications will be made to the nanoparticle to develop it as a radiosensitizer to allow for enhanced treatment in radiation therapy. The further elaboration of this study provides great potential toward the development of a theranostic agent for clinical applications.

4. EXPERIMENTAL SECTION

Materials: Silver Nitrate ($AgNO_3$), Pyrrole, Chitosan, Iron (III) Chloride ($FeCl_3$), (3-aminopropyl) triethoxysilane (APTES), 4-(*N*-Maleimidomethyl)cyclohexanecarboxylic acid *N*-hydroxysuccinimide ester (SMCC)(≥98%, powder), Dialysis Tubing benzoylated, Ammonium Hydroxide (NH_4OH), Nitric Acid (HNO_3) were purchased from (Sigma-Aldrich, St. Louis, MO) and used as received. Dulbecco's Modified Eagle's Medium (DMEM), L-glutamine, and RPMI medium were purchased from Life Technologies (Grand Island, NY). Fetal bovine serum (Atlanta Biologicals, Lawrenceville, GA) and the V7 ligand (Cisbio, Bedford, MA) were used as received.

Characterizations: The UV-vis absorption spectra were recorded with both MSOT and a Thermo-Scientific Model NanoDrop 2000 spectrophotometer. TEM images were obtained using a Tecnai-F20. Each TEM sample was prepared by dropping 50 µL of nanoparticle solution (in Milli-Q) on to copper-mesh grids (Electron Microscopy Science, Hatfield, PA) and they were then allowed to dry in room temperature overnight before imaging. For zeta-potential, the samples were measured by a Zetasizer Nano-ZS (Malvern Instruments

Ltd.) at room temperature. Smoluchowski's equation was used to determine the electrophoretic mobility (μE) of the sample:

$$\zeta = \frac{\eta}{\varepsilon}\mu_{\mathrm{e}}$$

The ζ stands for the zeta-potential, ε the existing permittivity of the solvent, and η the viscosity of solvent. The same Zetasizer Nano-ZS (Malvern Instruments Ltd.) was used to measure size distribution for Dynamic Light Scattering (DLS).

Preparation of Materials: Stir bars, spatulas, and beakers were cleaned and thoroughly rinsed with DI water and Ethanol, and were then placed in autoclave. Materials were allowed to cool before any reactants were added.

Synthesis of AgCl Core Solution: The additions and polymerizations of this preparation step occurred in a 5° C environment. 0.003g of $AgNO_3$ and 0.0083 mL of pyrrole were added to a 6.7 mL chitosan solution (1% weight in 0.05 M HNO_3). 0.047g of $FeCl_3$ was dissolved in 5 mL of Milli-Q water and the dispersion was then introduced to the chitosan solution. The resulting solution was polymerized for 12hrs. Once polymerization was completed, dialysis tubing was utilized to remove impurities from the mixture. Dialysis tubing was placed in a 0.05 M HNO_3 solution for an additional 12 hrs. Lastly, the AgCl core-shell material was obtained by a series of precipitation with acetone and centrifugation (4000 RPM for 25 min). Once the supernatant was removed, the precipitate was placed in a vacuum for 12 hrs at room temperature. The resulting product formed was the AgCl core-shell material.

Synthesis of PPy Hollow Nanosphere: A 0.005g portion of the AgCl core-shell material was dispersed in 20 mL of Milli-Q water by a combination of vortex and ultrasonication. The pH of the solution was adjusted to 12 by drop-wise addition of 5M NH_4OH and then stirred for 24 hrs in a 5° C environment. Dialysis tubing was used to remove the formed silver ammonia ions. This removal process occurred in a 0.1M NH_4OH solution. Once dialysis was completed, the pH of the solution was adjusted down to 4 with the drop-wise addition of 2M HNO_3. Finally, the PPy hollow nanospheres were obtained by a series of precipitation with acetone and centrifugation (4000 RPM for 30 min). Once the supernatant was removed, the precipitate was placed in a vacuum for 12 hrs at room temperature. The resulting product formed was the PPy hollow nanospheres.

Conjugation of V7-Ligand to PPy-CS Hollow Nanosphere: 0.0025 g of the solid PPy-CS material was obtained and placed in an Eppendorf tube containing 1 mL of phosphate buffer solution (PBS) containing a pH of 7.4. This solution was then dispersed by a series of vortex and ultrasonication. From the solution, 300 µL were placed in a separate Eppendorf tube and 30 µL of APTES were added and the mixture was vortexed for 30 min. Once finished, the pH of the solution was reduced down to 3.8 and 30 µL of IR-780 dye was introduced. The solution was then vortexed for 20 min. After this second round of vortex, the pH of the solution was readjusted back up to 7.4 with the drop-wise addition of NaOH and this resulting mixture was placed on vortex for 10 min. Next, 50 µL of SMCC (15 mM, 0.005014g in 1mL of DMF) was introduced to the solution and immediately after 50 µ of the V7-ligand (0.005g in 300 µL of DMF) was added as well. The Eppendorf was then vortexed for 12 hrs.

Cell Culture: The ovarian cell lines A2780 and ES-2 were cultured in DMEM medium (Life Technologies) with 10% FBS (Atlanta Biologicals) and 1% L-Glutamine (Life Technologies) at 37° C in a humidified atmosphere of 5% CO_2.

In Vitro Infrared Imaging to Determine pH-specificity: A2780 and ES-2 cells were placed in 6-well plates at a density of 500,000 cells per well. The 2 separate rows contained varying pH- media. One contained a pH of 6.6, whereas the other maintained a pH of 7.4. After 24 hrs of incubation at 37° C and non-CO_2, 50 µL of V7-conjugated PPy-CS hollow nanosphere (22.85 µM) was introduced to two of the columns for the A2780 and the ES-2 cells. The last column served as a control group. The cell-plates were placed on a rocker in the non-CO_2 incubator for 20 min; it was then placed on the Odyssey (LI-COR Biosciences) to determine if there was signaling present. Once signaling was detected, the cell-plates were washed with the corresponding phosphate buffer solution (PBS) and then placed back in to non-CO_2 incubator for an additional 20 min. The need for placement in a non-CO_2 environment stemmed from the desire to prevent side-reactions between the pH-specified phosphate buffer and the environmental carbon-dioxide. This process was repeated 3 times until optimal pH-specific signaling was achieved. Dosimetry analysis of IR-780 dye was conducted using Image-J software.

Optoacoustic Imaging of Tissue Phantoms: Tissue Phantoms (A mixture of agar and lipid used to mimic living tissue) provide an ideal model in allowing for comparable density and size found in mice. This model of imaging allows for an indicator of possible success *in vivo*. ES-2 cells were placed into 6-well plates for 24 hrs in DMEM media. After completion, the media were removed, pH-specific media were then applied and the cells were incubated for 4 hrs at 37°C in non-CO_2. The PPy-CS hollow nanospheres (50 µL) were then added to the wells and rocked in the incubator for an additional 2 hrs. Next, the cells underwent a series of 3 washes with specified PBS of pH 6.6 and 7.4 to each row. The cells were then scraped from each well and were collected in 1 mL of the corresponding PBS. Tissue phantoms were constructed with the use of Agar (Sigma Aldrich, St. Louis, MO), intralipid (Sigma Aldrich, St. Louis, MO), and DI water.

REFERENCES

1.Gurka, M.K., et al., *Identification of pancreatic tumors in vivo with ligand-targeted, pH responsive mesoporous silica nanoparticles by multispectral optoacoustic tomography.* Journal of Controlled Release, 2016.

2.Tietze, R., et al., *Magnetic nanoparticle-based drug delivery for cancer therapy.* Biochemical and biophysical research communications, 2015. **468**(3): p. 463-470.

3.Beziere, N., et al., *Dynamic imaging of PEGylated indocyanine green (ICG) liposomes within the tumor microenvironment using multi-spectral optoacoustic tomography (MSOT).* Biomaterials, 2015. **37**: p. 415-424.

4.Auffan, M., et al., *Chemical stability of metallic nanoparticles: a parameter controlling their potential cellular toxicity in vitro.* Environmental Pollution, 2009. **157**(4): p. 1127-1133.

5.Zhang, Y., K. Luo, and Z. Gu, *Functional Dendritic Polymer-Based Nanoscale Vehicles for Imaging-Guided Cancer Therapy*, in *Advances in Nanotheranostics I*. 2016, Springer. p. 271-299.

6.Cheng, D., H. Xia, and H.S.O. Chan, *Facile fabrication of AgCl@ polypyrrole-chitosan core-shell nanoparticles and polymeric hollow nanospheres.* Langmuir, 2004. **20**(23): p. 9909-9912.

7.Li, G., et al., *Polymeric hollow spheres assembled from ALG-g-PNIPAM and β-cyclodextrin for controlled drug release.* International journal of biological macromolecules, 2016. **82**: p. 381-386.

8.Geng, J., et al., *Conjugated Polymer and Gold Nanoparticle Co-loaded PLGA Nanocomposites with Eccentric Internal Nanostructure for Dual-modal Targeted Cellular Imaging.* Small, 2012. **8**(15): p. 2421-2429.

9.Wang, J., et al., *Enhanced Light Absorption in Porous Particles for Ultra-NIR-Sensitive Biomaterials.* ACS Macro Letters, 2015. **4**(4): p. 392-397.

10.Ntziachristos, V. and D. Razansky, *Molecular imaging by means of multispectral optoacoustic tomography (MSOT).* Chemical reviews, 2010. **110**(5): p. 2783-2794.

11.Ntziachristos, V., *Going deeper than microscopy: the optical imaging frontier in biology.* Nature methods, 2010. **7**(8): p. 603-614.

12.Ter-Pogossian, M.M., et al., *A Positron-Emission Transaxial Tomograph for Nuclear Imaging (PETT) 1.* Radiology, 1975. **114**(1): p. 89-98.

13.Brecht, H.-P., et al., *Whole-body three-dimensional optoacoustic tomography system for small animals.* Journal of biomedical optics, 2009. **14**(6): p. 064007-064007-8.

14.Kimbrough, C.W., et al., *Orthotopic pancreatic tumors detected by optoacoustic tomography using Syndecan-1.* J Surg Res, 2015. **193**(1): p. 246-54.

15.Hudson, S.V., et al., *Targeted noninvasive imaging of EGFR-expressing orthotopic pancreatic cancer using multispectral optoacoustic tomography.* Cancer Res, 2014. **74**(21): p. 6271-9.

16.Kimbrough, C.W., et al., *Targeting Acidity in Pancreatic Adenocarcinoma: Multispectral Optoacoustic Tomography Detects pH-Low Insertion Peptide Probes In Vivo.* Clin Cancer Res, 2015. **21**(20): p. 4576-85.

17.Razansky, D., A. Buehler, and V. Ntziachristos, *Volumetric real-time multispectral optoacoustic tomography of biomarkers.* Nature protocols, 2011. **6**(8): p. 1121-1129.

18.Taruttis, A., et al., *Fast multispectral optoacoustic tomography (MSOT) for dynamic imaging of pharmacokinetics and biodistribution in multiple organs.* PLoS One, 2012. **7**(1): p. e30491.

19.Kleinerman, R.A., *Cancer risks following diagnostic and therapeutic radiation exposure in children.* Pediatric radiology, 2006. **36**(2): p. 121-125.

20.Razansky, D., J. Baeten, and V. Ntziachristos, *Sensitivity of molecular target detection by multispectral optoacoustic tomography (MSOT).* Medical physics, 2009. **36**(3): p. 939-945.

21.Ntziachristos, V., et al., *Looking and listening to light: the evolution of whole-body photonic imaging.* Nature biotechnology, 2005. **23**(3): p. 313-320.

22.Mallidi, S., G.P. Luke, and S. Emelianov, *Photoacoustic imaging in cancer detection, diagnosis, and treatment guidance.* Trends Biotechnol, 2011. **29**(5): p. 213-21.

23.Wang, L.V. and S. Hu, *Photoacoustic tomography: in vivo imaging from organelles to organs.* Science, 2012. **335**(6075): p. 1458-62.

24.Luker, G.D. and K.E. Luker, *Optical imaging: current applications and future directions.* J Nucl Med, 2008. **49**(1): p. 1-4.

25.Senger, D.R., et al., *Tumor cells secrete a vascular permeability factor that promotes accumulation of ascites fluid.* Science, 1983. **219**(4587): p. 983-985.

26.Orimo, A., et al., *Stromal fibroblasts present in invasive human breast carcinomas promote tumor growth and angiogenesis through elevated SDF-1/CXCL12 secretion.* Cell, 2005. **121**(3): p. 335-348.

27.Rofstad, E.K., et al., *Acidic extracellular pH promotes experimental metastasis of human melanoma cells in athymic nude mice.* Cancer research, 2006. **66**(13): p. 6699-6707.

28.Švastová, E., et al., *Hypoxia activates the capacity of tumor-associated carbonic anhydrase IX to acidify extracellular pH.* FEBS letters, 2004. **577**(3): p. 439-445.

29.Dighiero, G., et al., *Autoantibody activity of immunoglobulins isolated from B-cell follicular lymphomas.* Blood, 1991. **78**(3): p. 581-585.

30.Gerweck, L.E. and K. Seetharaman, *Cellular pH gradient in tumor versus normal tissue: potential exploitation for the treatment of cancer.* Cancer research, 1996. **56**(6): p. 1194-1198.

31.Andreev, O.A., et al., *pH (low) insertion peptide (pHLIP) inserts across a lipid bilayer as a helix and exits by a different path.* Proceedings of the National Academy of Sciences, 2010. **107**(9): p. 4081-4086.

32.Yao, L., et al., *pHLIP peptide targets nanogold particles to tumors.* Proceedings of the National Academy of Sciences, 2013. **110**(2): p. 465-470.

33.Weerakkody, D., et al., *Family of pH (low) insertion peptides for tumor targeting.* Proceedings of the National Academy of Sciences, 2013. **110**(15): p. 5834-5839.

34.Zhao, Z., et al., *A Controlled-Release Nanocarrier with Extracellular pH Value Driven Tumor Targeting and Translocation for Drug Delivery.* Angewandte Chemie International Edition, 2013. **52**(29): p. 7487-7491.

35.Gao, W., J.M. Chan, and O.C. Farokhzad, *pH-responsive nanoparticles for drug delivery.* Molecular pharmaceutics, 2010. **7**(6): p. 1913-1920.

36.Jiang, S., et al., *Surface-functionalized nanoparticles for biosensing and imaging-guided therapeutics.* Nanoscale, 2013. **5**(8): p. 3127-3148.

37.Eghtedari, M., et al., *High sensitivity of in vivo detection of gold nanorods using a laser optoacoustic imaging system.* Nano letters, 2007. **7**(7): p. 1914-1918.

38.Chen, F. and Y. Zhu, *Chitosan enclosed mesoporous silica nanoparticles as drug nano-carriers: sensitive response to the narrow pH range.* Microporous and Mesoporous Materials, 2012. **150**: p. 83-89.

39.Bhattarai, N., J. Gunn, and M. Zhang, *Chitosan-based hydrogels for controlled, localized drug delivery.* Advanced drug delivery reviews, 2010. **62**(1): p. 83-99.

40.Huang, J., et al., *Effects of nanoparticle size on cellular uptake and liver MRI with polyvinylpyrrolidone-coated iron oxide nanoparticles.* ACS nano, 2010. **4**(12): p. 7151-7160.

41.Murdock, R.C., et al., *Characterization of nanomaterial dispersion in solution prior to in vitro exposure using dynamic light scattering technique.* Toxicological Sciences, 2008. **101**(2): p. 239-253.

42.Dobrovolskaia, M.A., et al., *Interaction of colloidal gold nanoparticles with human blood: effects on particle size and analysis of plasma protein binding profiles.* Nanomedicine: Nanotechnology, Biology and Medicine, 2009. **5**(2): p. 106-117.

43.Chorom, M. and P. Rengasamy, *Dispersion and zeta potential of pure clays as related to net particle charge under varying pH, electrolyte concentration and cation type.* European Journal of Soil Science, 1995. **46**(4): p. 657-665.

44.Butler, M. and D. Ginley, *Prediction of Flatband Potentials at Semiconductor-Electrolyte Interfaces from Atomic Electronegativities.* Journal of the Electrochemical Society, 1978. **125**(2): p. 228-232.

45.Shah, N.B., J. Dong, and J.C. Bischof, *Cellular uptake and nanoscale localization of gold nanoparticles in cancer using label-free confocal Raman microscopy.* Molecular pharmaceutics, 2010. **8**(1): p. 176-184.

46.Santra, S., et al., *Drug/Dye-Loaded, Multifunctional Iron Oxide Nanoparticles for Combined Targeted Cancer Therapy and Dual Optical/Magnetic Resonance Imaging.* small, 2009. **5**(16): p. 1862-1868.

47.Su, P.-G. and C.-P. Wang, *Flexible humidity sensor based on TiO 2 nanoparticles-polypyrrole-poly-[3-(methacrylamino) propyl] trimethyl ammonium chloride composite materials.* Sensors and Actuators B: Chemical, 2008. **129**(2): p. 538-543.

Figure Legend

Figure 1: A.) The silver-core portrayed by the silver circle is enclosed by a chitosan-coat depicted with the porous blue sphere. At pH of 6.6, V7 ligand became active and dye release was present. The protruding red-lines represent the active V7 ligand and the smaller circles depict cargo-release. At pH of 7.4, dye release was much less significant. B.) Transmission Electron Microscopy (TEM) images demonstrate the successful removal of the AgCl core to form the PPy-CS hollow nanospheres. The TEM images display the diameter of the PPy-CS hollow nanospheres as 43.56 $\pm$ 9 nm with a pore size of 15 $\pm$ 6 nm

Figure 2: Dynamic Light Scattering (DLS) measurement of PPy-CS hollow nanospheres demonstrate a size of 51.39 nm. This size is within the range depicted from the TEM imaging.

Figure 3: The conjugation of PPy-CS hollow nanospheres with chitosan. Zeta Potential confirms the presence of chitosan on the nanoparticle. This can be seen with the increase in pH with the corresponding decrease in voltage. This correlation is the result of lessened protonation on the chitosan coated PPy-CS hollow nanospheres

Figure 4: Multispectral optoacoustic tomographic (MSOT) image of the conjugated PPy-CS hollow nanosphere in phantom tissue displays distinct absorbance spectrum detected by MSOT system.

Figure 5: The absorbance spectrum for the PPy-CS hollow nanosphere was obtained. From phantom imaging, the pyrrole present in the particle exhibited a signal on its own without the aid of IR-780 dye.

Figure 6: A.) Odyssey Infrared Imaging displays distinct *in*-vitro cellular uptake in acidic cellular environment, pH 6.6, compared to that of pH7.4. B.) Odyssey images display a significant difference in the level of intensity of signal that was present between the PPy-CS hollow nanospheres in pH of 7.4 compared to that of pH 6.6.

Figure 7: During tissue phantom imaging, two samples were used to determine which procedure, for the addition of APTES, provided the greatest difference in signal between pH of 7.4 and 6.6. Both particle samples resulted in a difference in the signal intensity. However, the addition of APTES before the conjugation of SMCC and V7 displayed a greater difference in signal intensity compared to the addition of APTES along with the initial PPy-CS hollow nanospheres. APTES (First) displayed a difference of approximately 7 times more intensity for pH 6.6 compared to 7.4. APTES (Later) displayed a difference of approximately 9.4 times more intensity for pH 6.6 compared to 7.4.

Figure 8: PPy-CS hollow nanospheres loaded with IR-780 dye were evaluated for pH-specific dye release. The dye-conjugated nanoparticles were introduced into phosphate buffer saline (PBS) solutions of pH 6.6, 6.9, or 7.4. The absorbance level of each solution was measured by UV-Vis spectroscopy over a 10 hour period. It was determined that the level of absorbance directly correlated with the amount of IR-780 dye that had been released from the PPy-CS hollow nanospheres. The PPy-CS hollow nanospheres in PBS solution of pH 6.6 were found to have

released ~1.7 times greater the amount of IR-780 dye compared to those in PBS solution of pH 6.9 and 7.4. This contrast in dye release illustrates the effective pH-specificity found in the PPy-CS hollow nanospheres.